Hole-Transporting Host-Polymer Series Consisting of Triphenylamine Basic Structures for Phosphorescent Polymer Light-Emitting Diodes

MANUEL W. THESEN,[1] BIANCA HÖFER,[2] MARC DEBEAUX,[3] SILVIA JANIETZ,[1] ARMIN WEDEL,[1] ANNA KÖHLER,[2] HANS-HERMANN JOHANNES,[3] HARTMUT KRUEGER[1]

[1]Fraunhofer-Institut fuer Angewandte Polymerforschung, Wissenschaftspark Golm, Geiselbergstr. 69, D-14476 Potsdam, Germany

[2]Universität Bayreuth, Universitätsstr. 30, 95440 Bayreuth, Germany

[3]Labor für Elektrooptik am Institut für Hochfrequenztechnik, Technische Universität Braunschweig, Bienroder Weg 94, 38106 Braunschweig, Germany

Received 29 January 2010; accepted 10 May 2010
DOI: 10.1002/pola.24127
Published online in Wiley InterScience (www.interscience.wiley.com).

ABSTRACT: A series of novel styrene derived monomers with triphenylamine-based units, and their polymers have been synthesized and compared with the well-known structure of polymer of *N*,*N*′-bis(3-methylphenyl)-*N*,*N*′-diphenylbenzidine with respect to their hole-transporting behavior in phosphorescent polymer light-emitting diodes (PLEDs). A vinyltriphenylamine structure was selected as a basic unit, functionalized at the para positions with the following side groups: diphenylamine, 3-methylphenyl-aniline, 1- and 2-naphthylamine, carbazole, and phenothiazine. The polymers are used in PLEDs as host polymers for blend systems with the following device configuration: glass/indium–tin–oxide/PEDOT:PSS/polymer-blend/CsF/Ca/Ag. In addition to the hole-transporting host polymer, the polymer blend includes a phosphorescent dopant [Ir(Me-ppy)$_3$] and an electron-transporting molecule (2-(4-biphenyl)-5-(4-*tert*-butylphenyl)-1,3,4-oxadiazole). We demonstrate that two polymers are excellent hole-transporting matrix materials for these blend systems because of their good overall electroluminescent performances and their comparatively high glass transition temperatures. For the carbazole-substituted polymer (T_g = 246 °C), a luminous efficiency of 35 cd A^{-1} and a brightness of 6700 cd m^{-2} at 10 V is accessible. The phenothiazine-functionalized polymer (T_g = 220 °C) shows nearly the same outstanding PLED behavior. Hence, both these polymers outperform the well-known polymer of *N*,*N*′-bis(3-methylphenyl)-*N*,*N*′-diphenylbenzidine, showing only a luminous efficiency of 7.9 cd A^{-1} and a brightness of 2500 cd m^{-2} (10 V). © 2010 Wiley Periodicals, Inc. J Polym Sci Part A: Polym Chem 48: 3417–3430, 2010

KEYWORDS: charge transport; electroluminescence; fluorescence; host polymer; organic light-emitting diode

INTRODUCTION Polymer light-emitting devices (PLEDs) have inspired both researchers and investors since Burroughes et al.[1] reported the first discovery of a PLED in 1990. One remarkable advantage of polymers for light emission in displays is the ability to use simple and low-cost fabrication methods from solution, such as printing techniques. Large-area displays or plane lighting with light-emitting polymers fabricated via ink jet, stamp transfer, or roll-to-roll processes are now conceivable.[2–5] The physical effect of light emission can be divided into two different general phenomena, fluorescence and phosphorescence. Statistically, excitons in organic materials are created in a ratio of 1:3 for fluorescence to phosphorescence.[6] Thus, the light emission of a conjugated polymer, generated by fluorescence, is restricted by spin statistics to an efficiency of 25%, unless spin-dependent exciton recombination takes place.[7] These singlet emitting materials for PLED applications are mainly conjugated polymers, such as polyfluorene or poly(*p*-phenylenevinylene) derivatives.[8–12] With phosphorescent transition metal complexes carrying organic ligands, higher quantum efficiencies can be obtained in a light-emitting diode than with singlet emitting materials.[13] Some transition metal complexes, in the first instance iridium-(III) complexes, provide very short triplet lifetimes of excited states due to high radiative decay rates, so that up to 100% internal quantum efficiencies of these phosphorescent dopants in adapted matrices are possible.[14] Therefore, the higher luminous efficacy of phosphorescent dopants and the related increased energy efficiency compared with conjugated fluorescent polymers are the most promising advantages using triplets for light emission in PLEDs. Furthermore, the tuning of the phosphorescence emission wavelength across the visible spectrum is relatively easy by changing a ligand of the iridium complex system.[15,16] For an application of phosphorescent complexes in PLEDs, conjugated host polymers have been investigated. However, the interaction of fluorescence from the conjugated polymer with phosphorescence from the triplet dopand can cause several problems, in particular for devices that emit in the

Correspondence to: H. Krueger (E-mail: hartmut.krueger@iap.fraunhofer.de)
Journal of Polymer Science: Part A: Polymer Chemistry, Vol. 48, 3417–3430 (2010)

blue spectral range. Another possibility is the implementation of nonconjugated polymers, e.g., poly(*N*-vinylcarbazole) (PVK) or polystyrene to achieve full-color phosphorescent displays.[17,18] A comparatively simple approach for the preparation of single-layer devices is the use of a polymer blend system, whereas the active components are mixed into a polymer single layer. Highly efficient and bright PLEDs have been reported by blending a PVK-matrix with phosphorescent dopants, electron-, and additional hole-transporting molecules.[19–22] Following this idea, a phosphorescent dopant blended together with an electron and a hole transporting material can be considered as an emissive layer in a single-layer device. This approach opens an easy way to investigate new polymer charge transport materials for PLEDs. Therefore, the main interest, beside high-efficient phosphorescent dopants, has focused on the application of new charge-transporting materials. Arrays of hole-transporting small molecule materials have been reported, e.g., star-shaped molecules.[23–25] Charge-transporting materials have to meet a wide range of demands, primarily electronic characteristics in respect to efficiency and brightness, adaptable energy levels, high purity, availability, processability, high glass-transition temperatures, and a long-term stability.

Polystyrene is known to be a chemically stable and optically inert polymer. Therefore, Suzuki et al.[26] reported a polymer matrix system based on polystyrene with covalently fixed electron- and hole-transporting side functionalities. Further, to avoid phase separation and degradation during PLED operation, the phosphorescent complex was attached to the polystyrene backbone and for those systems external quantum efficiencies up to 12% were observed. Recently, we investigated the influence of a side-chain spacer separating the electronically active moieties, such as charge-transporting molecules and emitter, from the polystyrene backbone of the terpolymers.[27] Therefore, we built up PLEDs with these polymers and compared their performances with that one of the same polymers without these spacer moieties. It was concluded that energy transfer is favored in more compact polymer systems and that such transfer is suppressed when spacer moieties are introduced in polymers with a styrene backbone. Similarly, McKeown et al.[28] reported on polymer hole-transporting materials from substituted styrenes with a triarylamine basic structure tested with respect to their field-effect mobility in organic transistors. Furthermore, Debeaux et al.[29] published a new class of charge-transporting polymers based on phenylbenzoimidazole moieties used as electron-transporting material in a polymer blend system single-layer phosphorescent PLED. The novel polymer systems showed similar electronic behavior to the small molecule 1,3,5-tris(1-phenyl-1*H*-benzo[*d*]imidazol-2-yl)benzene.

Following this method, we established a series of novel hole-transporting monomers by attaching these materials directly at the polystyrene chain. In this work, we present the monomer and polymer syntheses and report on the electrochemical, optical, and electroluminescent behavior of the prepared polymers as host materials in blend systems with 2-(4-biphenyl)-5-(4-*tert*-butylphenyl)-1,3,4-oxadiazole (*tert*-BuPBD) as electron-transporting material and Ir(2-(4-tolyl)pyridinato)$_3$ [Ir(Me-ppy)$_3$] as phosphorescent dopant. The blends are investigated with respect to their electroluminescent behavior in single-layer PLEDs. Finally, we report on the electrochemical and optical characteristics of these polymer materials and compare the results with the well-known polymer of *N*,*N*′-bis(3-methylphenyl)-*N*,*N*′-diphenylbenzidine (poly(TPD)).

EXPERIMENTAL

Materials and Methods

All materials were obtained from Aldrich Chemical Company (Munich, Germany) or Acros Organics (Geel, Belgium) and used without any further purification unless otherwise stated. Silica gel 60 (Merck) (Darmstadt, Germany) was used in the separation and purification of compounds by column chromatography. Solvents for column chromatography, recrystallization, and purification were received from Th. Geyer GmbH (Berlin, Germany) and J. T. Baker (Deventer, Netherlands). Dry solvents were received from Aldrich Chemical Company, stored over molecular sieve and sealed under an inert atmosphere.

Procedure for activation of copper: Copper (10 g, dendritic) was stirred in 100 mL acetone with 2% of iodine for 10 min. The suspension was filtered and washed with acetone, stirred for another 5 min in a mixture of 100 mL acetone and 100 mL conc. HCl, filtered, and washed again with acetone until neutrality. The activated copper was dried under reduced pressure at 80 °C.

Thin-layer chromatography (TLC) was done with ALUGRAM SIL G/UV$_{254}$ TLC plates on aluminum from Macherey-Nagel. Reverse-phased TLC was done with RP-18 F$_{254s}$ TLC plates on aluminum from Merck.

High-resolution (500 MHz) ^{1}H-NMR and ^{13}C-NMR (125 MHz) spectra were recorded on a UNITY INOVA 500 spectrometer from Varian at room temperature.

Elemental analyses were obtained using a Thermo Scientific FlashEA 1112 CHNS/O Automatic Elemental Analyzer.

Gel-permeation chromatography (GPC) at 25 °C in tetrahydrofuran (THF) has been applied to determine the molecular weights. For this purpose, a combination of Waters HPLC-Pump 515, Autosampler 717 plus, Dual λ Absorbance Detector 2487, and a Refrative Index Detector 2414 has been used. A precolumn and three columns from Waters (7.8 mm $\times$ 300 mm; Styragel HR3, HR4, HR5) filled with a copolymer of styrene and divinylbenzene 5 μm and PS-Standards from Polymer Laboratories (Varian) were used. The polymer solutions (2 mg L^{-1} in THF) stirred for 24 h at room temperature and filtered through a 1-μm syringe PTFE filter before 2 $\times$ 100 μL of each polymer solution were injected. Molecular weights were calculated with the Empower software from Waters.

Thermal analysis was performed with differential scanning calorimetry using a Netzsch DSC 204 with a scanning rate of 10 K min^{-1}.

For UV/vis and photoluminescence spectra, about 100-nm-thick films were spun at 900 rpm from toluene solutions

(for **8a**, **8b**, **8c**, and **8e**) or THF solutions (for **8d** and **8f**, because of poor solubility in toluene) (concentrations 20 g L^{-1}) onto silica glass substrates. Absorption was measured using a Carry 5000 UV/vis spectrometer. During the photoluminescence measurements, the samples were held in a continuous flow He cryostat and measured under vacuum (for steady-state measurements) or in a small background pressure of He (for temperature-dependent time-resolved measurements). The temperature was recorded with an Oxford Temperature controller ITC 502. For time-resolved measurements, excitation was provided by the frequency tripled output of a Nd:YAG laser at 355 nm with a pulse duration of about 10 ns. A home-built electronic shutter was used to reduce the excitation frequency from the 10 Hz repetition rate of the laser to 0.2 Hz. For the steady-state spectra, the 355 and 364 nm lines of an Ar^+ laser were used as an excitation source. The emission was detected with a CCD camera Andor iDus coupled to an Oriel spectrograph MSH201 (for steady-state spectra) or with a gated intensified ICCD camera Andor iStar coupled to an Oriel spectrograph MS257 (for time-resolved detection). Measurements of the photoluminescence quantum yields of the hosts were carried out using the integrating sphere technique.[30]

Photoelectron spectroscopy was applied for the estimation of the HOMO energy levels using a Riken Keiki AC-2. The investigated polymers were measured as powder stored in stainless steel crucibles.

IR spectra were recorded of the solids on a Digilab Scimitar FTS2000 FT-IR spectrometer equipped with a Golden Gate Mk II ATR-System from Specac.

Cyclovoltammetric Measurements

Voltammograms were obtained on an EG and G Parc model 273 potentiostat. A three-electrode configuration was applied, contained in an undivided cell consisting of a glassy carbon electrode (area 0.5 cm^2) in which the polymer film was deposited, a platinum mesh as the counter electrode and an Ag/AgCl (3 M NaCl and sat. AgCl) as a reference electrode. Bu_4NBF_4 (0.1 M) in acetonitrile was used as an electrolyte, and prior each measurement the electochemical cell has been deoxygenated with nitrogen. The electrochemical cell was calibrated by the use of a ferrocene standard and the ferrocene half-wave potential has been estimated to be 435 mV for this assembly. Polymer solutions (1 wt %) in $CHCl_3$ were prepared and 5 μL were deposited on the glassy carbon electrode. The prepared electrodes were kept under vacuum and dried at 60 °C for 2 h.

Device Fabrication

The transparent indium–tin–oxide-covered glass slides were received from OPTREX Europe GmbH (sheet resistance 20 Ω/□) and were chemically wet cleaned in an ultra sonic bath before further processing. The hole injecting layer was polyethylenedioxythiophene doped with polystyrenesulphonic acid (PEDOT:PSS, CH8000, H.C. Starck) and dried at temperatures above 130 °C for 5 min to remove the residual solvent. Followed by a spin-coating process the emitting polymer-blend solution was deposited from chlorobenzene to receive polymer layer thicknesses of about 70 to 90 nm after another annealing step for 10 min at 110 °C. The polymer-blend solutions (62 wt % polymer, 30 wt % *tert*-BuPBD, 8 wt % $Ir(Me\text{-}ppy)_3$; the phosphorescent dopant received from American Dye Source, Inc., were dissolved in chlorobenzene for 24 h at room temperature using a shaker before the polymer solutions were filtrated through polytetrafluoroethylene PTFE-syringe filters with pore sizes of 0.1 μm. The cathodes (CsF 4 nm; Ca 15 nm; Ag 50 nm) were assembled by a thermal evaporation process at pressures below 10^{-5} Pa. Four devices of each polymer were built to guarantee uniformity. The complete sample preparation and measurements have been investigated under an inert atmosphere.

Device Characterization

The current–voltage and the luminance–voltage characteristics of the devices were measured simultaneously with a computer-controlled Keithley 236 Source-Measure-Unit in combination with an Optometer Model GO352 equipped with a calibrated sensor head for the luminance measurements. The electroluminescence spectra were recorded with a diode-array spectrometer EPP 2000 from Stella Net Inc.

Field Effect Transistors

The organic field effect transistor (OFET) structures prepared were of a "bottom gate"-configuration using heavily doped Si-wafers as substrates and common gate electrodes. The gate dielectric was thermally grown directly on the wafer SiO_2 of thickness 230 nm and capacitance 14.6 nF cm^{-2}. On the top of SiO_2, the source and drain electrodes (Au) were deposited using a photolithographic technique (L = 10 μm, W = 195 mm). The wafers were carefully cleaned with several solvents, dried under a nitrogen flow, and treated with hexamethyldisiloxane. Finally, the active polymer layers were spin-coated from chloroform or chlorobenzene/chloroform (1:1) solutions with polymer concentrations of 7 to 10 g L^{-1} under inert atmospheric conditions. Before electrical characterization, the samples were annealed in inert atmosphere for 5 min at 100 °C. The OFET characteristics were measured in dark under glove box conditions, using two Source-Measure Units 236 combined with a Trigger-Control Unit 2361 and Metrics Software (all three items Keithley Instruments).

Synthesis

Monomer Synthesis

***4*-[N,N-*Di(4-iodophenyl)amino)benzaldehyde (2)* [*28*].** Yield 96%, mp 143–144 °C. ^{1}H NMR (500 MHz, $CDCl_3$, δ, ppm): 9.84 (s, 1H, CHO), 7.71 (d, J = 8.8, 2H), 7.28 (d, J = 8.8, 4H), 7.06 (d, J = 8.8, 2H), 6.89 (d, J = 8.8, 4H). IR (ATR, cm^{-1}): ν = 3058, 3036, 3006 (w, C—H aromatic), 2794, 2715, (w, C—H aldehyde), 1685 (m, C=O), 1676 (m). Anal. calcd for $C_{19}H_{13}I_2NO$ (M_w 525.12 g mol^{-1}): C 43.46, H 2.50, N 2.67, O 3.05; found C: 43.34, H 2.49, N 2.70, O 3.17.

***General Technique I: 4-{*N,N-*Bis[4-(*N,N-*diphenylamino) phenyl]amino}benzaldehyde (3a)*.** To simplify matters, the reaction procedures for **3b–f** were calculated in regard to the reaction **3a**. In the following, a factor is given in the form of eq x.xx to represent the equimolar factor between diphenylamine as amine in reaction **3a** to the similar

reactions with the other amines for the reactions **3b–f**. Compound **2** 5.00 g (9.52 mmol), 9.67 g (57.1 mmol) of diphenylamine as amine, 10.53 g (76.2 mmol) of K_2CO_3, 3.67 g (57.1 mmol) of activated copper bronze (see above), and 0.50 g (1.90 mmol) 18-crown-6 were weighed into a reaction flask with a septum. The apparatus was deoxygenized by an evacuation-flushing process with Ar which was repeated three times and 50 mL of dry *o*-dichlorobenzene were injected via the septum. The mixture was stirred 48 h at reflux temperature, cooled to room temperature afterward, filtered, and concentrated using a rotatory evaporator. Column chromatography with toluene led to 4.40 g (76%) of the pure product as a slight yellow glass. ^{1}H NMR (500 MHz, $CDCl_3$, δ, ppm): 9.79 (s, 1H, CHO), 7.68 (d, J = 8.6, 2H), 7.27 (m, 10H), 7.13 (m, 8H), 7.04 (m, 8H), 7.02 (m, 4H). R_f = 0.41 (toluene). IR (ATR, cm^{-1}): ν = 3059, 3034, 3008 (w, C—H aromatic), 2806, 2715 (w, C—H aldehyde), 1688 (m, C=O). Anal. calcd for $C_{43}H_{33}N_3O$ (M_w 607.74 g mol^{-1}): C 84.98, H 5.47, N 6.91, O 2.63; found: C 84.42, H 5.47, N 6.69, O 2.98.

***4-(*N,N-*Bis{4-[*N,N-*phenyl(*m-*tolyl)amino]phenyl}amino) benzaldehyde* (*3b*).** Using the general technique I (eq 1.00) with 3-methyl-*N*-phenylaniline as amine and similar other reactants, followed by column chromatography with toluene, 2.74 g (45%) of the pure product as a slight yellow glass were obtained. ^{1}H NMR (500 MHz, $CDCl_3$, δ, ppm): 9.78 (s, 1H, CHO), 7.67 (d, J = 8.6, 2H), 7.25 (m, 4H), 7.16 (t, J = 7.8, 2H), 7.11 (d, J = 8.6, 4H), 7.04 (m, 12H), 6.92 (m, 4H), 6.68 (d, J = 8.6, 2H), 2.28 (s, 3H). ^{13}C NMR (125 MHz, $CDCl_3$, δ, ppm): 190.05 (1C, CHO), 153.32 (1C, ArC_q), 147.36 (2C, ArC_q), 147.16 (2C, ArC_q), 144.91 (2C, ArC_q), 139.55 (2C, ArC_q), 138.98 (2C, ArC_q), 131.11 (2C, ArCH), 129.02 (4C, ArCH), 128.89 (2C, ArCH), 128.01 (1C, ArC_q), 126.92 (4C, ArCH), 125.00 (2C, ArCH), 124.05 (4C, ArCH), 123.99 (4C, ArCH), 123.85 (2C, ArCH), 122.62 (2C, ArCH), 121.56 (2C, ArCH), 117.70 (2C, ArCH). R_f = 0.45 (toluene). IR (ATR, cm^{-1}): ν = 3059, 3034, 3008 (w, C—H aromatic), 2920, 2853 (w), 2808, 2729 (w, C—H aldehyde), 1688 (m, C=O). Anal. calcd for $C_{45}H_{37}N_3O$ (M_w, 635.79 g mol^{-1}): C 85.01, H 5.87, N 6.61, O 2.52; found: C 84.24, H 5.99, N 6.31, O 3.12.

***4-(*N,N-*Bis{4-[*N,N-*phenyl(1-naphthyl)amino]phenyl}amino) benzaldehyde* (*3c*).** Using the general technique I (eq 0.28) with 1-naphthylamine as amine and similar other reactants, followed by column chromatography with toluene, 1.11 g (59%) of the pure product as slight a yellow glass was obtained. ^{1}H NMR (500 MHz, $CDCl_3$, δ, ppm): 9.75 (s, 1H, CHO), 7.95 (d, J = 8.6, 2H), 7.89 (m, J = 8.3, 2H), 7.78 (d, J = 8.3, 2H), 7.63 (m, J = 8.8, 2H), 7.48 (m, 4H), 7.37 (m, 4H), 7.20 (m, 4H), 7.05 (m, 4H), 6.98 (m, 8H), 6.94 (m, 4H). ^{13}C NMR (125 MHz, $CDCl_3$, δ, ppm): 190.28 (1C, CHO), 153.64 (1C, ArC_q), 148.03 (2C, ArC_q), 145.74 (2C, ArC_q), 143.17 (2C, ArC_q), 139.18 (2C, ArC_q), 135.29 (2C, ArC_q), 131.34 (2C, ArC_q), 131.21 (2C, ArCH), 129.16 (4C, ArCH), 128.46 (2C, ArCH), 128.06 (1C, ArC_q), 127.31 (2C, ArCH), 127.23 (4C, ArCH), 126.70 (2C, ArCH), 126.47 (2C, ArCH), 126.36 (2C, ArCH), 126.21 (2C, ArCH), 124.10 (2C, ArCH), 122.44 (4C, ArCH), 121.88 (2C, ArCH), 121.81 (4C, ArCH), 117.62 (2C, ArCH). R_f = 0.41 (toluene). IR (ATR, cm^{-1}): ν = 3059, 3034, 3008 (w, C—H aromatic), 2814, 2729 (w, C—H aldehyde), 1686 (m, C=O). Anal. calcd for $C_{51}H_{37}N_3O$ (M_w 707.86 g mol^{-1}): C 86.53, H 5.27, N 5.94, O 2.26; found: C 85.56, H 5.90, N 5.21, O 2.43.

***4-(*N,N-*Bis{4-[*N,N-*phenyl(2-naphthyl)amino]phenyl}amino) benzaldehyde* (*3d*).** Using the general technique I (eq 1.00) with 2-naphthylamine as amine and similar other reactants, followed by column chromatography with toluene, 2.75 g (41%) of the pure product as a slight yellow glass was obtained. ^{1}H NMR (500 MHz, $CDCl_3$, δ, ppm): 9.80 (s, 1H, CHO), 7.75 (t, J = 9.1, 4H), 7.69 (d, J = 8.8, 2H), 7.62 (d, J = 7.8, 2H), 7.47 (s, 2H), 7.38 (m, 4H), 7.31 (m, 6H), 7.18 (d, J = 7.8, 4H), 7.10 (m, 8H), 7.06 (m, 4H). ^{13}C NMR (125 MHz, $CDCl_3$, δ, ppm): 190.30 (1C, CHO), 153.45 (1C, ArC_q), 147.48 (2C, ArC_q), 145.10 (2C, ArC_q), 144.94 (2C, ArC_q), 140.25 (2C, ArC_q), 143.36 (2C, ArC_q), 131.39 (2C, ArC_q), 130.15 (2C, ArCH), 129.40 (4C, ArCH), 129.04 (2C, ArCH), 128.46 (1C, ArC_q), 127.58 (2C, ArCH), 127.21 (4C, ArCH), 126.93 (2C, ArCH), 126.35 (2C, ArCH), 124.66 (2C, ArCH), 124.64 (4C, ArCH), 124.57 (4C, ArCH), 124.46 (2C, ArCH), 123.27 (2C, ArCH), 120.64 (2C, ArCH), 118.22 (2C, ArCH). R_f = 0.46 (toluene). IR (ATR, cm^{-1}): ν = 3059, 3034, 3008 (w, C—H aromatic), 2806, 2723 (w, C—H aldehyde), 1690 (m, C=O). Anal. calcd for $C_{51}H_{37}N_3O$ (M_w 707.86 g mol^{-1}): C 86.53, H 5.27, N 5.94; found: C 85.23, H 5.27, N 5.88.

N,N-*Bis[4-(carbazolyl)phenyl]benzaldehyde* (*3e*). Using the general technique I (eq 2.40) with carbazole as amine (double amount) and similar other reactants, followed by column chromatography with toluene, 8.16 g (59%) of the pure product as a slight yellow glass was obtained. ^{1}H NMR (500 MHz, $CDCl_3$, δ, ppm): 9.90 (s, 1H, CHO), 8.16 (d, J = 7.8 Hz, 4H), 7.83 (d, J = 8.6 Hz, 2H), 7.60 (d, J = 8.6 Hz, 4H), 7.52–7.42 (m, 12H), 7.33–7.27 (m, 6H). R_f = 0.50 (toluene). IR (ATR, cm^{-1}): ν = 3045, 3021, 3008 (w, C—H aromatic), 2712, 2688 (w, C—H aldehyde), 1687 (m, C=O). Anal. calcd for $C_{43}H_{29}N_3O$ (M_w 603.71 g mol^{-1}): C 85.55, H 4.84, N 6.96, O 2.65; found: C 84.76, H 4.70, N 7.07, O 2.87.

***4-{Bis[4-(phenothiazinyl)phenyl]amino}benzaldehyde* (*3f*).** Using the general technique I (eq 0.80) with phenothiazine as amine and similar other reactants, followed by column chromatography with toluene, 3.00 g (59%) of the pure product as a slight yellow glass was obtained. ^{1}H NMR (500 MHz, CD_2Cl_2, δ, ppm): 9.89 (s, 1H, CHO), 7.81 (d, J = 8.6, 2H), 7.38 (m, 8H), 7.24 (m, 2H), 7.08 (m, 4H), 6.96 (m, 4H), 6.88 (m, 4H), 6.42 (d, J = 8.3, 4H). R_f = 0.50 (toluene). IR (ATR, cm^{-1}): ν = 3061, 3034, 3008 (w, C—H aromatic), 2828, 2729 (w, C—H aldehyde), 2691, 1734 (w), 1688 (m, C=O). Anal. calcd for $C_{34}H_{29}N_3OS_2$ (M_w 667.84 g mol^{-1}): C 77.33, H 4.38, N 6.29; found: C 78.30, H 4.64, N 5.69.

***4-{*N,N-*Bis[4-(*N,N-*diphenylamino)phenyl]amino}vinylphenyl* (*4a*).** A total of 1.24 g (3.46 mmol) $MePPh_3Br$ was weighed into a reaction flask with septum and the apparatus was deoxygenized by an evacuation-flushing process with Ar which was repeated three times. Fifteen milliliters of dry toluene was added and the solution was cooled to 0 °C. A total of 2.16 mL (3.46 mmol) of *n*-BuLi (1.6 M in hexane) was

injected slowly and the reaction mixture stirred for 20 min at 0 °C. Two grams (3.29 mmol) of the benzaldehyde derivative **3a** was dissolved in 20 mL of dry toluene and added slowly to the reaction mixture. The mixture was stirred for another 20 min at 0 °C and over night at room temperature afterward. The mixture was diluted with CH_2Cl_2, washed several times with water, dried over Na_2SO_4, filtrated, and concentrated. Recrystallization from toluene/EtOH 2:1 gave 0.64 g (32%) of the pure product as beige crystals (mp 197–199 °C). ^{1}H NMR (500 MHz, THF-d_8, δ, ppm): 7.28 (d, J = 8.6, 2H), 7.20 (m, 8H), 7.05 (d, 8H), 6.99 (m, 8H), 6.94 (m, 6H), 6.63 (dd, J = 10.7, 17.6, 1H, CH_2=CHAr), 5.60 (d, J = 17.6, 1H, CH_2=CHAr *trans*), 5.06 (d, J = 10.7, 1H, CH_2=CHAr *cis*). R_f = 0.59 (hexane/ethyl acetate 10:1), 0.61 (THF/MeOH/H_2O 8:8:1). IR (ATR, cm^{-1}): ν = 3085 (w, C—H vinyl), 3061, 3034, 3008 (w, C—H aromatic), 2979 (w, C—H vinyl), 1624 (w, C=C vinyl). Anal. calcd for $C_{44}H_{35}N_3$ (M_w 605.77 g mol^{-1}): C 87.24, H 5.82, N 6.94; found: C 87.25, H 6.09, N 6.85.

***General Technique II: 4-(*N,N*-Bis{4-[N,N-phenyl(*m*-tolyl)amino]phenyl}amino)vinylphenyl* (*4b*).** To simplify matters, the reaction procedures for **4c–f** and **7** were calculated in regard to the reaction **4b**. In the following, a factor is given in the form of (eq x.xx) to represent the equimolar factor between the reaction **4b** with **3b** as aldehyde to the similar reactions with the other aldehydes for the reactions **4c–f** and **7**. A total of 0.58 g (5.14 mmol) of KO^{t}Bu and 1.70 g (4.77 mmol) of $MePPh_3Br$ were weighed into a reaction flask with a septum. The apparatus was deoxygenized by an evacuation-flushing process with Ar for three times. Twenty milliliters of dry THF was added and the solution was cooled to 0 °C and stirred for 20 min. Two grams (3.15 mmol) of the benzaldehyde derivative **3b** were dissolved in 10 mL of dry THF and injected slowly. The reaction mixture was stirred at 0 °C for 1 h. CH_2Cl_2 were added, the solution was washed with H_2O, dried over Na_2SO_4, filtrated, and concentrated. Recrystallization from CH_2Cl_2/EtOH 1:2 led to 1.42 g (71%) of the pure product as a beige solid (mp 185–189 °C). ^{1}H NMR (500 MHz, THF-d_8, δ, ppm): 7.28 (d, J = 8.6, 2H), 7.19 (m, 4H), 7.11 (t, J = 7.8, 2H), 7.01 (m, 12H), 6.93 (m, 6H), 6.84 (d, J = 7.8, 2H), 6.79 (d, J = 7.3, 2H), 6.63 (dd, J = 10.7, 17.6, 1H, ArC*H*=CH_2), 5.60 (d, J = 17.6, 1H, CH_2=CHAr *trans*), 5.06 (d, J = 10.7, 1H, CH_2=CHAr *cis*). ^{13}C-NMR (^{125}MHz, $CDCl_3$, δ, ppm): 148.90 (2C, ArC_q), 148.68 (2C, ArC_q), 148.48 (1C, ArC_q), 144.04 (2C, ArC_q), 143.30 (2C, ArC_q), 139.66 (2C, ArC_q), 137.23 (1C, vinyl CH), 132.26 (1C, ArC_q), 129.80 (4C, ArCH), 129.72 (2C, ArCH), 127.74 (2C, ArCH), 125.98 (4C, ArCH), 125.86 (4C, ArCH), 125.42 (2C, ArCH), 124.34 (4C, ArCH), 124.24 (2C, ArCH), 123.22 (2C, ArCH), 122.96 (2C, ArCH), 122.06 (2C, ArCH), 111.60 (1C, vinyl CH_2). R_f = 0.58 (hexane/ethyl acetate 10:1), 0.53 (THF/MeOH/H_2O 8:8:1). IR (ATR, cm^{-1}): ν = 3084 (w, C—H vinyl), 3061, 3034, 3008 (w, C—H aromatic), 2976 (w, C—H vinyl), 1627 (w, C=C vinyl). Anal. calcd for $C_{46}H_{39}N_3$ (M_w 633.82 g mol^{-1}): C 87.17, H 6.20, N 6.63; found: C 86.79, H 6.34, N 6.40.

***4-(*N,N*-Bis{4-[N,N-phenyl(1-naphthyl)amino]phenyl}amino)vinylphenyl* (*4c*).** Using the general technique II (eq 0.31) with the benzaldehyde derivative **3c**, followed by a recrystallization from CH_2Cl_2/EtOH 1:2, 0.54 g (77%) of the pure product was obtained as beige crystals (mp 220–223 °C). ^{1}H NMR (500 MHz, THF-d_8, δ, ppm): 7.95 (d, J = 8.3, 2H), 7.87 (d, J = 8.1, 2H), 7.76 (d, J = 8.3, 2H), 7.44 (t, J = 7.8, 2H), 7.41 (t, J = 7.8, 2H), 7.32 (m, 4H), 7.23 (d, 2H), 7.11 (m, 4H), 6.93 (m, 14H), 6.82 (t, J = 7.3, 2H), 6.60 (dd, J = 10.7, 17.6, 1H, ArC*H*=CH_2), 5.57 (d, J = 17.6, 1H, CH_2=CHAr *trans*), 5.03 (d, J = 10.7, 1H, CH_2=CHAr *cis*). ^{13}C NMR (125 MHz, $CDCl_3$, δ, ppm): 149.52 (2C, ArC_q), 148.59 (1C, ArC_q), 144.74 (2C, ArC_q), 144.43 (2C, ArC_q), 142.75 (2C, ArC_q), 137.25 (1C, vinyl CH), 136.39 (2C, ArC_q), 132.16 (2C, ArC_q), 131.92 (1C, ArC_q), 129.66 (4C, ArCH), 129.10 (2C, ArCH), 127.74 (2C, ArCH), 127.65 (2C, ArCH), 127.06 (2C, ArCH), 127.00 (2C, ArCH), 126.89 (2C, ArCH), 126.75 (2C, ArCH), 126.10 (4C, ArCH), 124.90 (2C, ArCH), 124.15 (4C, ArCH), 122.72 (2C, ArCH), 121.79 (2C, ArCH), 121.66 (4C, ArCH),111.34 (1C, vinyl CH_2). R_f = 0.47 (hexane/ethyl acetate 10:1), 0.51 (THF/MeOH/H_2O 8:8:1). IR (ATR, cm^{-1}): ν = 3086 (w, C—H vinyl), 3058, 3040, 3004 (w, C—H aromatic), 2977 (w, C—H vinyl), 1627 (w, C=C vinyl). Anal. calcd for $C_{52}H_{39}N_3$ (M_w 705.89 g mol^{-1}): C 88.48, H 5.57, N 5.95; found: C 87.03, H 5.81, N 5.64.

***4-(*N,N*-Bis{4-[N,N-phenyl(2-naphthyl)amino]phenyl}amino)vinylphenyl* (*4d*).** Using the general technique II (eq 0.63) with the benzaldehyde derivative **3d**, followed by a recrystallization from CH_2Cl_2/EtOH 1:2, 1.21 g (86%) of the pure product was obtained as beige crystals (mp 268–270 °C). ^{1}H NMR (500 MHz, THF-d_8, δ, ppm): 7.71 (m, 4H), 7.58 (d, J = 7.8, 2H), 7.42 (s, 2H), 7.28 (m, 12H), 7.11 (d, 4H), 7.04 (m, 10H), 6.98 (d, 2H), 6.64 (dd, J = 10.7, 17.6, 1H, ArC*H*=CH_2), 5.62 (d, J = 17.6, 1H, CH_2=CHAr *trans*), 5.07 (d, J = 10.7, 1H, CH_2=CHAr *cis*). ^{13}C-NMR (125 MHz, $CDCl_3$, δ, ppm): 148.78 (2C, ArC_q), 148.41 (1C, ArC_q), 146.36 (2C, ArC_q), 143.87 (2C, ArC_q), 143.70 (2C, ArC_q), 137.23 (1C, vinyl CH), 135.55 (2C, ArC_q), 132.49 (1C, ArC_q), 131.04 (2C, ArC_q), 129.97 (4C, ArCH), 129.57 (2C, ArCH), 128.16 (2C, ArCH), 127.80 (2C, ArCH), 127.58 (2C, ArCH), 126.85 (2C, ArCH), 126.20 (4C, ArCH), 126.04 (4C, ArCH), 125.02 (2C, ArCH), 124.75 (6C, ArCH), 123.45 (4C, ArCH), 120.57 (2C, ArCH), 111.70 (1C, vinyl CH_2). R_f = 0.57 (hexane/ethyl acetate 10:1), 0.59 (THF/MeOH/H_2O 8:8:1). IR (ATR, cm^{-1}): ν = 3085 (w, C—H vinyl), 3058, 3036, 3004 (w, C—H aromatic), 2985 (w, C—H vinyl), 1627 (w, C=C vinyl). Anal. calcd for $C_{52}H_{39}N_3$ (M_w 705.89 g mol^{-1}): C 88.48, H 5.57, N 5.95; found: C 87.89, H 5.52, N 5.92.

***N,N-Bis[4-(carbazolyl)phenyl]-4-vinylaniline* (*4e*).** Using the general technique II (eq 2.47) with the benzaldehyde derivative **3e**, followed by a recrystallization from toluene/EtOH 1:1, 2.80 g (60%) of the pure product was obtained as colorless crystals (mp 169–171 °C). ^{1}H NMR (500 MHz, DMSO-d_6, δ, ppm): 8.25 (d, J = 7.7 Hz, 4H), 7.60 (d, J = 8.7 Hz, 4H), 7.54 (d, J = 8.6 Hz, 2H), 7.48–7.43 (m, 8H), 7.40 (d, J = 8.7 Hz, 4H), 7.32–7.23 (m, 6H), 6.75 (dd, J = 17.6, 11.0 Hz, 1H, ArC*H*=CH_2), 5.79 (d, J = 17.6 Hz, 1H, CH_2=CHAr *trans*), 5.24 (d, J = 11.0 Hz, 1H, CH_2=CHAr *cis*). R_f = 0.63 (hexane/ethyl acetate 10:1), 0.43 (THF/MeOH/H_2O 8:8:1). IR (ATR, cm^{-1}): ν = 3085 (w, C—H vinyl), 3062,

3044, 3006 (w, C—H aromatic), 1625 (w, C=C vinyl). Anal. calcd for $C_{44}H_{31}N_3$ (M_w 601.74 g mol^{-1}): C 87.82, H 5.19, N 6.98; found: C 87.61, H 5.29, N 6.95.

N,N-*Bis[4-(phenothiazinyl)phenyl]-4-vinylaniline (4f)*. Using the general technique II (eq 0.71) with the benzaldehyde derivative **3f**, followed by a recrystallization from toluene/EtOH 1:1, 0.92 g (62%) of the pure product were obtained as colorless crystals (mp 145–148 °C). ^{1}H NMR (500 MHz, THF-d_8, δ, ppm): 7.45 (d, 2H), 7.39 (d, 4H), 7.22 (d, 4H), 7.25 (d, 2H), 6.97 (d, 4H), 6.87 (t, 4H), 6.78 (t, 4H), 6.72 (dd, J = 10.7, 17.6, 1H, ArC*H*=CH$_2$), 6.37 (d, 4H), 5.72 (d, J = 17.6, 1H, CH$_2$=CHAr *trans*), 5.17 (d, J = 10.7, 1H, CH$_2$=CHAr *cis*). R_f = 0.61 (hexane/ethyl acetate 10:1), 0.57 (THF/MeOH/H$_2$O 8:8:1). IR (ATR, cm^{-1}): ν = 3085 (w, C—H vinyl), 3061, 3038, 3006 (w, C—H aromatic), 2976 (w, C—H vinyl), 1627 (w, C=C vinyl). Anal. calcd for $C_{44}H_{31}N_3S_2$ (M_w 665.87 g mol^{-1}): C 79.37, H 4.69, N 6.31, S 9.63; found: C 79.05, H 4.71, N 6.02, S 9.40.

***4-((4′-(Phenyl(*m*-tolyl)amino)biphenyl-4-yl)(*m*-tolyl)amino) benzaldehyde* (6).** The apparatus was evacuated and flushed with Ar three times. Twenty milliliters of dry DMF was added and cooled to 0 °C. A total of 2.17 mL (23.8 mmol) of freshly distilled $POCl_3$ was injected and the mixture was stirred for 30 min at 0 °C. Ten grams (19.4 mmol) of TPD was dissolved in 20 mL of DMF and injected into the reaction mixture. The mixture was heated to 80 °C and stirred for 2 h, while a change in the color from slight yellow to brown was observed. The reaction mixture was allowed to cool to room temperature and slowly added to 500 mL of 1 M Na_2CO_3 (aq.). The green precipitate was filtered off, dissolved in CH_2Cl_2, washed with H_2O, dried over Na_2SO_4, filtered again, and concentrated. The brown oily residue was purified by column chromatography with toluene to obtain 4.85 g (46%) of pure **6** as a slight yellow glass. ^{1}H NMR (500 MHz, $CDCl_3$, δ, ppm): **6a** (27%): 9.81 (s, 1H, CHO), 7.69 (d,2H, J = 8.3), 7.53 (d, 2H, J = 8.3), 7.46 (d, 2H, J = 8.3), 7.26 (t, 2H, J = 7.6), 7.19 (m, 9H), 7.12 (d, 4H, J = 8.1), 7.03 (m, 1H), 6.96 (s, 1H), 6.93 (d, 1H, J = 8.1), 6.86 (d, 1H, J = 7.6), 2.32 (s, 3H), 2.28 (s, 3H); **6b** (73%): 10.06 (s, 1H, CHO), 7.62 (d, 1H, J = 8.5), 7.53 (d, 2H, J = 8.3), 7.46 (d, 2H, J = 8.3), 7.35 (t, 2H, J = 7.8), 7.26 (t, 2H, J = 7.6), 7.19 (m, 4H), 7.12 (d, 4H, J = 8.1), 7.03 (m, 3H), 6.96 (s, 1H), 6.93 (d, 1H, J = 8.1), 6.90 (d, 1H, J = 8.5), 6.86 (d, 1H, J = 7.6), 6.81 (s, 1H), 2.54 (s, 3H), 2.28 (s, 3H). R_f = 0.45 (toluene). IR (ATR, cm^{-1}): ν = 3060, 3031, 3007 (w, C—H aromatic), 2923, 2858 (w), 2839, 2730 (w, C—H aldehyde), 1735, 1682 (m, C=O). Anal. calcd for $C_{39}H_{32}N_2O$ (M_w 544.68 g mol^{-1}): C 86.00, H 5.92, N 5.14; found: C 85.57, H 6.13, N 5.05.

N-*Phenyl*-N,N′-*di*[*m*-*tolyl*-*N*′-*(4-vinylphenyl)]biphenyl-4,4′-diamine (7). Using the general technique II (eq 2.69) with the benzaldehyde derivative **6**, after column chromatography with toluene, 3.80 g (83%) of **7** was obtained as a colorless solid (mp 85–88 °C). ^{1}H NMR (500 MHz, $CDCl_3$, δ, ppm): **7a** (25%): 7.44 (d, 4H, J = 8.3), 7.30 (d, 1H, J = 8.3), 7.25 (m, 4H), 7.16 (m, 2H), 7.11 (m, 8H), 7.02 (m, 2H), 6.92 (m, 4H), 6.65 (dd, 1H, CH$_2$=CHAr, J = 10.7, 17.6), 5.64 (d, 1H, CH$_2$=CHAr *trans*, J = 17.6), 5.16 (d, 1H, CH$_2$=CHAr *cis*, J = 10.7), 2.35 (s, 3H); **7b** (75%): 7.44 (d, 4H, J = 8.3), 7.39 (d, 1H, J = 8.3), 7.25 (m, 4H), 7.16 (m, 2H), 7.11 (m, 6H), 7.02 (m, 2H), 6.92 (m, 4H), 6.85 (m, 2H), 6.91 (dd, 1H, CH$_2$=CHAr, J = 10.7, 17.6), 5.58 (d, 1H, CH$_2$=CHAr *trans*, J = 17.6), 5.21 (d, 1H, CH$_2$=CHAr *cis*, J = 10.7), 2.27 (s, 3H). IR (ATR, cm^{-1}): ν = 3084 (w, C—H vinyl), 3061, 3031 (w, C—H aromatic), 2970 (w, C—H vinyl). Anal. calcd for $C_{40}H_{34}N_2$ (M_w 542.71 g mol^{-1}): C 88.52, H 6.31, N 5.16; found: C 88.31, H 6.43, N 4.71.

Polymer Synthesis

***General Technique III: Poly*-[4-{N,N-*bis[4-(N,*N*-diphenylamino)phenyl]amino}vinylphenyl] (8a).** The monomer concentration was set to be 100 g l^{-1} in freshly distilled THF and 2 mol % *N,N*-azobisisobutyronitrile was selected as an initiator. The reaction was carried out in a glove box system under nitrogen atmosphere at 50 °C for 60 h. The resulting solution was allowed to cool to room temperature and demonomerized by repeated precipitation into a mixture of MeOH/Et$_2$O 2:1. The residue were dissolved again in THF and filtered through a syringe PTFE filter 0.2 μm. The solvent was removed *in vacuo* and the solution precipitated again into MeOH/Et$_2$O 2:1. The residue was filtered by the use of PTFE filters pore size 0.45 μm. The polymer was dried for 30 h at 80 °C *in vacuo*. Yield 76%. IR (ATR, cm^{-1}): ν = 3061, 3034, 3008 (w, C—H aromatic), 2919 (w, C—H aliphatic). T_g = 168 °C. λ_{max} (CHCl$_3$) = 308 nm. Anal. calcd for $[C_{44}H_{35}N_3]_n$: C 87.24, H 5.82, N 6.94; found: C 86.63, H 5.85, N 7.08.

***Poly*-[4-[N,N-*bis{4-*[N,N-*phenyl(*m*-tolyl)amino]phenyl}amino) vinylphenyl] (8b).** Using the general technique III, yield 65%. IR (ATR, cm^{-1}): ν = 3059, 3034, 3008 (w, C—H aromatic), 2919 (w, C—H aliphatic). T_g = 141 °C. λ_{max} (CHCl$_3$) = 316 nm. Anal. calcd for $[C_{46}H_{39}N_3]_n$: C 87.17, H 6.20, N 6.63; found: C 86.78, H 6.17, N 6.67.

***Poly*-[4-{N,N-*bis[4-*(N,N-*phenyl(1-naphthyl)amino]phenyl} amino]vinylphenyl] (8c).** Using the general technique III, yield 68%. IR (ATR, cm^{-1}): ν = 3058, 3036, 3007 (w, C—H aromatic), 2925, 2917 (w, C—H aliphatic). T_g = 173 °C. λ_{max} (CHCl$_3$) = 331 nm. Anal. calcd for $[C_{52}H_{39}N_3]_n$: C 88.48, H 5.57, N 5.95; found: C 87.61, H 5.58, N 6.07.

***Poly*-[4-{N,N-*bis[4-(*N,N-*phenyl(2-naphthyl)amino]phenyl} amino]vinylphenyl] (8d).** Using the general technique III, yield 75%. IR (ATR, cm^{-1}): ν = 3062, 3042, 3014 (w, C—H aromatic), 2918 (w, C—H aliphatic). T_g = 158 °C. λ_{max} (CHCl$_3$) = 326 nm. Anal. calcd for $[C_{52}H_{39}N_3]_n$: C 88.48, H 5.57, N 5.95; found: C 87.51, H 5.53, N 5.97.

***Poly-[*N,N-*Bis[4-(carbazolyl)phenyl]-4-vinylaniline]* (8e).** Using the general technique III, yield 85%. IR (ATR, cm^{-1}): ν = 3062, 3045, 3012 (w, C—H aromatic), 2919 (w, C—H aliphatic). T_g = 246 °C. λ_{max} (CHCl$_3$) = 324 nm. Anal. calcd for $[C_{44}H_{31}N_3]_n$: C 87.45, H 5.90, N 6.65; found: C 87.07, H 5.22, N 7.15.

***Poly-[*N,N-*Bis[4-(phenothiazinyl)phenyl]-4-vinylaniline]* (8f).** Using the general technique III, yield 75%. IR (ATR, cm^{-1}): ν = 3058, 3035, 3007 (w, C—H aromatic), 2922,

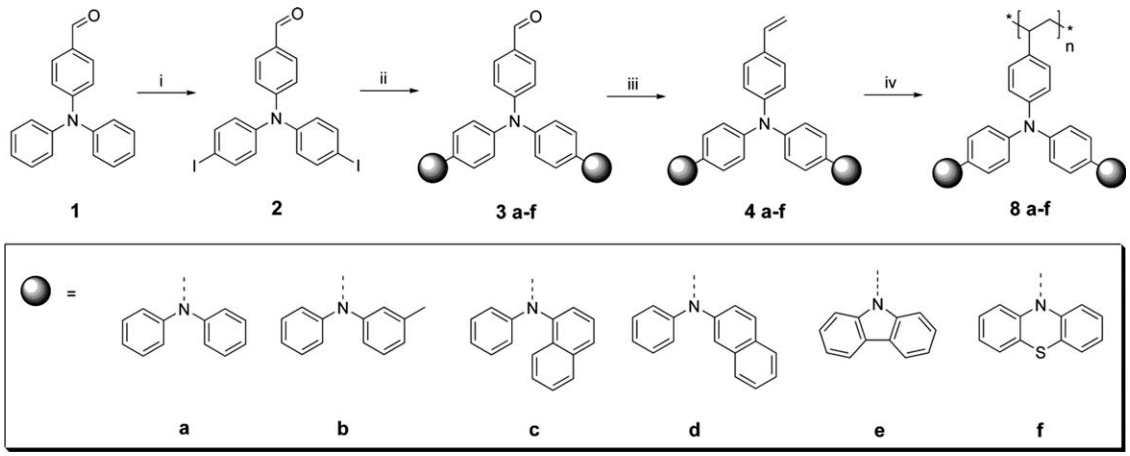

FIGURE 1 Synthesized hole-transporting polymers **8a–f**. Reagents and conditions: (i) CH_3COOH, H_2O 10:1, KI, KIO_3, 3 h, 80 °C—**2** (ii) K_2CO_3, activated Cu-Bronze, 18-crown-6, 1,2-dichlorobenzene, amine **a–f** (*N*,*N*-diphenylamine **a**, 3-Methyl-*N*-phenylaniline **b**, *N*-phenyl-1-naphthylamine **c**, *N*-phenyl-2-naphthylamine **d**, carbazole **e**, phenothiazine **f**), 48 h, 180 °C—**3a–f**. (iii) *n*-BuLi, $MePPh_3Br$, THF, 2 h, 0 °C; **4a**, KO^tBu, $MePPh_3Br$, THF, 2 h, 0 °C—**4b–f**. (iv) THF, AIBN, 50 °C, 60 h—**8a–f**.

2917 (w, C—H aliphatic). T_g = 220 °C. λ_{max} ($CHCl_3$) = 312 nm. Anal. calcd for $[C_{44}H_{31}N_3S_2]_n$: C 79.37, H 4.69, N 6.31, S 9.63; found: C 78.36, H 4.48, N 6.12, S 9.51.

***Poly*-[N-*phenyl*-N,N′-*Di*(m-*tolyl*-*N*′-*(4-vinylphenyl))bi-phenyl-4,4′-diamine]* (*9*).** Using general technique III, yield 55%. IR (ATR, cm^{-1}): ν = 3059, 3029, 3007 (w, C—H aromatic), 2920 (w, C—H aliphatic). T_g = 171 °C. λ_{max} ($CHCl_3$) = 354 nm. Anal. calcd for $[C_{40}H_{34}N_2]_n$: C 88.52, H 6.31, N 5.16; found: C 87.83, H 6.39, N 5.32.

RESULTS AND DISCUSSION

Monomer Syntheses

We followed a synthetic route introduced by McKeown et al.[28] for the monomer syntheses. The reaction scheme used for all synthesized monomers is displayed in Figure 1. The first step was the halogenation of 4-(diphenylamino)-benzaldehyde (**1**) with potassium iodine and potassium iodate in a 10:1 mixture of acetic acid and water to obtain compound **2**. Ullmann reaction with the selected amine (compound **a-f**) followed by a Wittig reaction with potassium *tert*-butylate (KO^tBu) and methyltriphenylphosphonium bromide ($MePPh_3Br$) in THF leads to the vinyl-functionalized monomers **4b–f** with good yields. Monomer **4a** was synthesized with *n*-butyl lithium as a base for the preparation of the respective phosphonium yield. This reagent turned out to be rather detrimental because of the low yield (only 30%) in the last reaction step and many undesirable side products, which are difficult to separate from the target structure. Therefore, subsequent reactions were carried out using KO^tBu for the preparation of the monomers **4b–f**, followed by a yield increase to approximately 70%.

The synthesis of the reference monomer, introduced by Suzuki et al., based on a TPD structure is shown in Figure 2. The first reaction step was a Vilsmeier formylation of TPD with phosphorus oxychloride in *N*,*N*-dimethylformamide to obtain the aldehyde derivative **6**. Suzuki et al. published an isomeric mixture of 28% **6a** and 72% **6b**. ^1H NMR spectroscopy confirmed a mixture of 27% **6a** and 73% **6b** for our product. The final step was a Wittig reaction with KO^tBu and $MePPh_3Br$ in THF to obtain the isomeric mixture of the final vinyl-functionalized monomer **7a/b** in a ratio of 1:3.

Polymerizations

The polymerizations were carried out in a glove box system under nitrogen atmosphere, whereas THF acts as solvent while the initiator was *N*,*N*′-azobisisobutyronitrile. The poly-

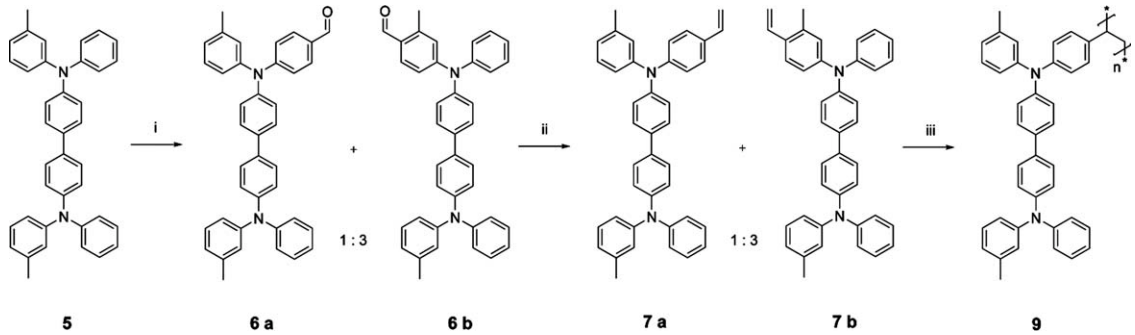

FIGURE 2 Synthesized hole-transporting polymer **9** (mixture of two implemented isomers **7a/b**). Reagents and conditions: DMF, $POCl_3$, 2 h, 80 °C—**6a/b**. $MePPh_3Br$, KO^tBu, 2h, 0 °C—**7a/b**. (iii) THF, AIBN, 50 °C, 60 h—**9**.

TABLE 1 Overview on Analytical Data of Polymers **8 a–f** and **9**

	Polymer						
	8a	**8b**	**8c**	**8d**	**8e**	**8f**	**9**
Approximate yield in %	76	65	68	75	85	75	55
GPC in 10^3 g mol^{-1}							
M_n	18.3	15.6	9.5	10.5	41.2	9.8	12.9
M_w	33.4	26.5	21.7	23.6	197.7	26.1	24.6
PDI	1.82	1.70	2.28	2.24	4.80	2.54	1.90
DSC in °C (T_g)	168	141	173	158	246	220	171

merization temperature was 50 °C for 60 h. Table 1 gives an overview of the polymer analyses data. The approximate yield of all polymerizations was about 70%. On one hand the phenyl-functionalized polymers **8a**, **8b**, and **9** present with polydispersity indices (PDIs) of about 1.8 reasonably narrow molecular weight distributions for free-radical polymerization processes. In contrast, the polymers with phenyl-naphthyl-functionalities and the polymer with the phenothiazine side group show quite higher PDIs of approximately 2.4, which can be mainly attributed to a poor monomer solubility observed in THF, especially for the naphthylamino-functionalized monomers. The maximum quotient between the weight average molar mass M_w and the number average molar mass M_n is obtained for polymer **8e**, with the carbazole units, which has a very high PDI of 4.80. The solubility of the carbazole-monomer in THF is quite good, so the high PDI may be due to a different origin. We observed a bimodular distribution in the size exclusion chromatogram of this polymer, so the comparatively high PDI of 4.80 may possibly be caused by the Norrish-Trommsdorff effect or chain-transfer mechanisms themselves.

For the glass transition temperatures (T_g), the phenyl-substituted polymers show the lowest T_g with 168 °C for the non-substituted and 141 °C for the methylene-substituted polymer, where this difference is caused by the additional methyl groups. Furthermore, the 1- and 2-naphthyl-derived polymers exhibit a difference of 15 K in the glass transition temperatures on their part, mainly caused by the higher flexibility of the 2-naphthyl side groups compared with the 1-substitution. Nevertheless, it has to be mentioned that the relatively small molecular weights of polymers **8c** and **8d** suggest that the measured T_g is not yet independent of the molecular weight, i.e., with similar molecular weights of **8c** and **8d** compared with the other polymers, a higher T_g should be observable. However, polymer **9** is in the same range with a T_g of 171 °C. The carbazole-substituted **8e** (246 °C) and the polymer with phenothiazine side groups **8f** (220 °C) present the highest T_gs. Comparing the structures of these two polymers **8e** and **8f** with that of **8a**, it is obvious that the glass transition temperature is much higher, which is caused by the stiffening C—C and C—S bonds, respectively, between the aromatic rings. In **8a** all three amine bonds are free in rotation, whereas in the case of the carbazole and the phenothiazine side groups the nitrogen is absolutely fixed, resulting overall in a stiffening of the polymer chain. Additionally, the carbazole shows an absolutely planar structure, whereas the phenothiazine is slightly twisted at the C—S bonds, i.e., the carbazole perform a better packaging and a more compact polymer chain, resulting in the higher T_g compared with that one of phenothiazine.

Spectroscopic and Electrochemical Investigation

The optical behavior of the synthesized polymers was studied in spin-coated solid films on silica glass substrates and in chloroform solutions. The UV/vis data of the films and chloroform solutions are summarized in Table 2, along with the 10K phosphorescence lifetimes and 0-0 peak positions and the 300K solid-state quantum yields. Only small shifts in a normal range between the maxima in solid film compared with those in solution are observable for all polymers.

To identify the singlet and triplet excited states formed in the compounds after excitation, we have performed spectroscopic measurements on thin films. Figure 3(a) shows the room temperature spectra of absorption and photoluminescence for continuous wave excitation. We observe a difference between the emission spectra of compounds **8c** and **8d** compared with the spectra of **8a**, **8b**, **8e**, and **8f**. The latter all show two peaks centered at about 3.0 eV (≈410 nm) and 2.5 eV (≈500 nm) for **8a**, **8b**, and **8e**, and at 2.6 eV (≈475 nm) and 2.1 eV (≈590 nm), respectively, for **8f**. In contrast, the spectra of **8c** and **8d** show only one broad emission peak centered at about 2.5 eV. In absorption, the difference is less pronounced. We notice a slightly lower energy onset of absorption at about 3.0 eV for **8c** and **8d** compared with about 3.2–3.3 eV (≈375–390 nm) for the other compounds.

The photoluminescence spectra are investigated in more detail in Figure 3(b) in which time-dependent emission spectra at 10 K are shown. The spectra were taken at delay times of 50 ns (solid line) and 500 ns (dotted line) after an excitation pulse. For both delay times, the gate width of the detector was 80 ms, i.e., any long-lived signal was collected. Although only the long-lived component was recorded with a delay time of 500 ns, in the measurement with 50 ns delay time possible short-lived components are added.

As in the steady-state room temperature spectra, we observe a high-energy band with little structure that is centered roughly at about 2.9 eV (≈430 nm) for compounds **8a**, **8b**, and **8e**, and at about 2.6 eV (≈475 nm) for **8c**, **8d**, and **8f**.

TABLE 2 Optical and Electrochemical Properties of Polymers **8a–f** and **9**

	Polymer						
	8a	**8b**	**8c**	**8d**	**8e**	**8f**	**9**
Absorption maximum[a] (nm)	308	316	331	326	324	312	354
Absorption maximum[b] (nm)	321	321	333	330	325	315	356
Absorption maximum[b] (eV)	3.86	3.86	3.72	3.76	3.82	3.94	3.48
Luminance Quantum Yield[c] (%)	4.0	7.5	4.5	10.0	5.0	0.5	
LUMO[d] (eV)	1.93	1.93	2.16	1.97	2.08	2.16	2.32
HOMO (CV)[e] (eV)	5.04	5.07	5.07	5.12	5.40	5.28	5.32
HOMO (AC-2)[f] (eV)	5.07	5.08	5.06	4.98	5.41	5.41	5.40
Optical Bandgap[g] (eV)	3.14	3.15	2.90	3.01	3.33	3.25	3.08
0-0 Peak of Phosphorescence (eV)	2.59	2.60	2.25	2.30	2.70	2.40	
Phoshorescence Lifetime[h] (ms)	256	235	123	268	228	65	

[a] In $CHCl_3$ solution.
[b] As solid film.
[c] ±1%.
[d] LUMO-energy levels were calculated by the use of UV/vis data
[e] Cyclovoltammetry.
[f] Photoelectron spectroscopy.
[g] Obtained from the onset of absorption.
[h] At 10 K.

This band disappears for a delay time of 500 ns and is therefore assigned to fluorescence.

At 10 K, there is an additional low-energy band with a well-resolved vibrational structure. The 0–0 peaks of the low-energy band are at about 2.6–2.7 eV for **8a**, **8b**, and **8e** and at about 2.2–2.4 eV for **8c**, **8d**, and **8f** (see Table 2 for exact values). This low-energy band is present at both delay times, although for compounds **8c** and **8d**, it is difficult to discern in the long red tail of the emission spectra taken at 50 ns.

To clarify the origin of this band, we measured its decay as a function of time (Fig. 4). The photoluminescence decays can be fitted by a single exponential yielding lifetimes of tens and hundreds of milliseconds (see Table 2). On the basis of the long lifetime and the vibrational structure, we assign the well-resolved low-energy emission at 10 K to phosphorescence.

We note the difference in vibrational structure between the fluorescence and the phosphorescence bands. This implies a different electronic origin for the singlet and the triplet state.

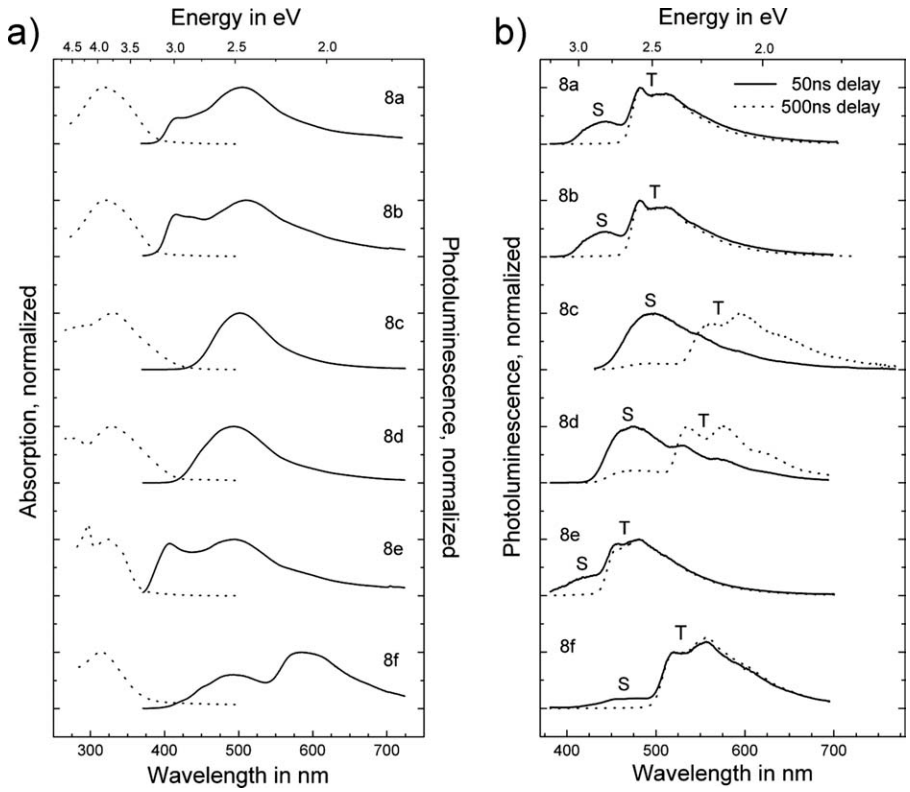

FIGURE 3 (a) Absorption (dotted line) and steady state photoluminescence (PL) (solid line) spectra at room temperature on solid films; (b) solid film photoluminescence (PL) spectra at 10 K, at a delay of 50 ns (solid line) and 500 ns (dotted line) after the laser pulse. T and S denote the assignment to triplet and singlet excited states, respectively.

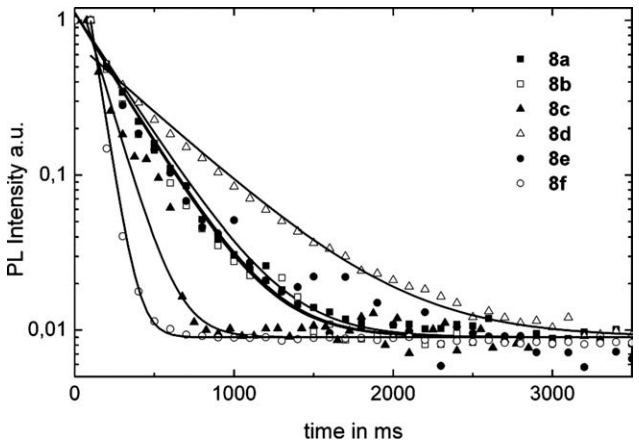

FIGURE 4 Decay of the photoluminescence intensity with time in thin films at 10 K.

For example, it is conceivable for the singlet state to have n–π^* or intramolecular charge-transfer character, both leading to little vibrational structure, while the well-resolved vibrational structure suggests that the triplet state might originate from a transition with a predominant π–π^* character. Since the exchange energy for a π–π^* transition tends to be larger than that for a n–π^* or intramolecular charge-transfer transition, an energetic arrangement of states in the order $^1(\pi$–$\pi^*)$, ^{1}(n–π^* or CT state), ^{3}(n–π^* or CT state), $^3(\pi$–$\pi^*)$ is highly possible.[7] While this might be the case in these compounds, quantum chemical calculations are required to clarify this.

We now consider the triplet lifetimes of the compounds in more detail. Compounds **8a**, **8b**, and **8e** only differ in the choice of an additional CH_3 sidegroup (**8b**) or a stiffening link (**8e**), so it is natural for the spectroscopic behavior and the measured lifetimes to be very similar. Accordingly, the overall luminescence quantum yields of **8a** and **8e** are essentially the same, 4 $\pm$ 1% and 5 $\pm$ 1%, respectively. The quantum yield of **8e** is higher (7.5 $\pm$ 1%), consistent with the higher luminous efficiency of LEDs made with **8b** as host compared with **8a** [Fig. 6(b)]. This points to a beneficial effect of the CH_3 sidegroup in suppressing detrimental intermolecular interactions. In the 10 K lifetime, this difference is not manifested since diffusion to sites with interchain interactions is usually frozen out at such low temperatures.[7]

In compound **8f**, the addition of the sulfur atom results in an overall bathochromic shift of the excited states and a strongly reduced lifetime for the triplet state. The lifetime of **8f** is only half the lifetime of **8c**, even though the triplet state in **8c** is at lower energy. Clearly, the short lifetime of 65 ms cannot be attributed merely to the slightly lower triplet energy according to the energy gap law.[31] Rather it seems that the introduction of the sulfur atom introduces some additional nonradiative or radiative decay channels. The emission from **8f** is weak and borders on the detection limit of our quantum efficiency measurement setup. From this, we infer that the decay route introduced by the incorporation of the sulfur atom to the chemical structure is of an undesired nonradiative type.

In a similar manner, the shorter lifetime of **8c** compared with **8d** along with the lower luminescence quantum yield also suggests a more effective nonradiative decay. It is well known that the triplet state in naphthalene compounds loses its energy very efficiently and nonradiatively via the high-energy C—H stretching vibrations.[32] Furthermore, naphthalene has its transition dipole moment along the short axis of the molecule. Consequently, the attachment of the naphthalene moiety to the amine in **8c** along the naphthalene short axis on the 1-position allows for an efficient coupling of the electronic transition to the C—H stretching vibration, in contrast to electron redistribution that is associated with the transition in **8d**. This is further confirmed by quantum chemical calculations of the electron wave functions on the basis of AM1/ZINDO (Austin Model 1/Zerner Intermediate neglect of differential overlap).

We now compare the spectra observed for compounds **8c** and **8d** with those of **8a**, **8b**, **8e** and **8f**. At 10 K, the emission from the two naphthalene-containing polymers is similar to that of the other compounds except for an overall bathchromic shift. This suggests that conjugation continues reasonably well through the nitrogen atoms resulting in more extended conjugated systems for the compounds with the naphthalene moieties in **8c** and **8d** compared with the compounds with only a short "phenyl" moiety attached, as in **8a**, **8b**, **8e**, and **8f**. To account for the difference in the room temperature steady-state spectra, i.e., the lack of a second emission band in **8c** and **8d**, more detailed spectroscopic investigations are required that are beyond the scope of this study.

In addition to the excited state energies, the positions of the frontier molecular orbitals are relevant for hole-transporting materials. Hole injection takes place from the anode into the highest occupied molecular orbital (HOMO). The HOMO energy levels of the polymers were investigated by photoemission spectroscopy of the polymer powder and verified by cyclovoltammetric investigations as solid films on a glassy carbon electrode. Overall, the HOMO energy levels of the polymers obtained with both methods are in a good agreement. We derived the optical bandgap from the solid film absorption spectra and calculated the LUMO by the use of the HOMO measured via photoelectron spectroscopy. LUMO, HOMO, and bandgap values are listed in Table 2 and displayed in Figure 5.

The structurally very similar phenylamino-substituted polymers **8a** and **8b** have nearly identical oxidation and reduction potentials. Comparison of **8a** with **8c** shows the modification from a phenyl group to a naphthalene group leaving the HOMO almost unchanged. Comparing the mesomeric structures of the two polymers **8c** and **8d** with the naphthalene groups, **8c** with the naphthalene in 1-position exhibits more mesomeric structures retaining full aromaticity than structure **8d** with the naphthalene connected in 2-position. As a result, the larger conjugated system **8c** has a somewhat reduced LUMO and bandgap.

When the two phenyl rings are stiffened by a C–C link to form a carbazole as in **8e,** the conjugation in this planar ring

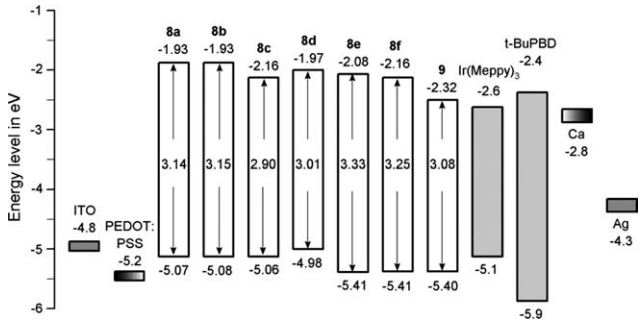

FIGURE 5 Measured HOMO, calculated LUMO energy levels, and calculated optical bandgaps of polymers **8a–f** and **9**.

system is enhanced compared with **8a**. It was found that two clearly separated energy levels are present at −5.41 and −5.74 eV measured by photoelectron spectroscopy. This result was further verified by cyclovoltammetric and the "higher" level is used as potential HOMO energy level in the following discussion. For polymer **8e**, the first oxidation potential is not very distinct in the measured photoelectron spectrum. The insertion of a sulfur atom in **8f** leads to a hypsochromic shift in the absorption maximum and the sulfur atom is responsible for a higher electron density in the attached molecule. Furthermore, the phenothiazine has a disturbed planar structure, the molecule is slightly angulated at the sulfur atom, whereas, the carbazole unit is strictly planar. This angle decreases the conjugation in the phenothiazine moiety. Comparison with literature shows a very good accordance between the measured energy levels of these polymers to those of small molecules with structural similarity, for example (**8b**[33], **8c**[34], **8d**[35], **8d**[36], and **9**[37]).

In conclusion, the measured HOMO energy levels of these investigated host polymer materials should allow the development of efficient phosphorescent PLEDs. Therefore, we decided to test PLEDs with our polymers as hole-transporting host materials, Ir(Me-ppy)$_3$ (HOMO −5.1 eV and LUMO −2.6 eV)[38] as phosphorescent dopant and *tert*-BuPBD as electron-transporting material (HOMO −5.9 eV and LUMO −2.4 eV).[39] In case of **8e**, **8f**, and **9**, with the lower HOMO, compared with the other polymers, a more efficient hole transfer to the emitter (HOMO −5,1 eV) should be possible.

Device Characterization

Single-layer phosphorescent PLEDs were prepared with these hole-transporting polymers in a configuration of (glass/indium–tin–oxide/PEDOT:PSS/polymer-blend/CsF/Ca/Ag) to compare the influence of different host-polymers on the electroluminescence properties of the device. In addition to the hole-transporting host-polymers, the blends consisted of 30 wt % *tert*-BuPBD as the electron-transporting material and of 8 wt % Ir(Me-ppy)$_3$ as the phosphorescent dopant. The electroluminescent behavior of the green emitting phosphorescent PLEDs are summarized in Table 3 and displayed in Figure 6. The electroluminescence spectra of the single-layer devices are illustrated in Figure 7 and the maxima of emission are further noted in Table 3.

In the electroluminescence spectrum, devices made with the host **8a**, **8b**, **8e**, and **8f** show essentially the same emission than the device made with the TPD host **9**, except that the shoulder at 550 nm has a little more intensity for **8a** and **8e**. Because of the energetic position and vibrational structure, we attribute this emission band to the expected phosphorescence from the Ir(Me-ppy)$_3$ guest. For the hosts **8c** and **8d**, the onset of emission still coincides with the Ir(Me-ppy)$_3$ guest emission; however, the emission peaks are shifted bathochromically, the spectra are broadened, and they show a tail extending to longer wavelengths. This observation points to a contribution from a state at lower energy such as an exciplex or electroplex. The latter denotes an exciplex state that is only formed for electrical excitation. To distinguish between exciplex and electroplex formation, we compare in Figure 7(c) the photoluminescence from a blend of the hosts **8c** with Ir(Me-ppy)$_3$ and **8d** with Ir(Me-ppy)$_3$ with the electroluminescence of corresponding devices. The red emission feature is not present for optical excitation of the blend, it only appears for electrical excitation. The long red tail observed in devices made with **8c** and **8d** can therefore be attributed to electroplex formation. Such electroplex emission is usually inefficient due to the low oscillator strength of such a charge-transfer-type state, and this may account for the poor performance of the LEDs made from **8c** and **8d** with respect to luminous efficiency or brightness.[32]

In addition to this, we note that in our spectroscopic analysis (Fig. 3), we find the 0–0 peak of the 10 K phosphorescence

TABLE 3 Electroluminescent Characteristics of Polymer-Blend PLEDs of **8a–f** and **9**

	Polymer						
	8a	**8b**	**8c**	**8d**	**8e**	**8f**	**9**
Layer thickness (nm)	86	96	83	83	93	74	87
Luminous efficiency[a] (cd A^{-1})	18.5	12.3	0.5	0.5	32.8	29.0	7.9
Current density[a] (mA cm^{-2})	21	16	29	22	12	12	21
Luminous efficiency[b] (cd A^{-1})	9.4	16.7	0.5	0.5	35.1	28.2	8.7
Brightness[c](cd m^{-2})	5000	4200	200	150	6700	6100	2600
Electroluminescence maximum (nm)	517	519	545	539	522	520	515

[a] At 8 V.
[b] At 100 cd m^{-2}.
[c] At 10 V.

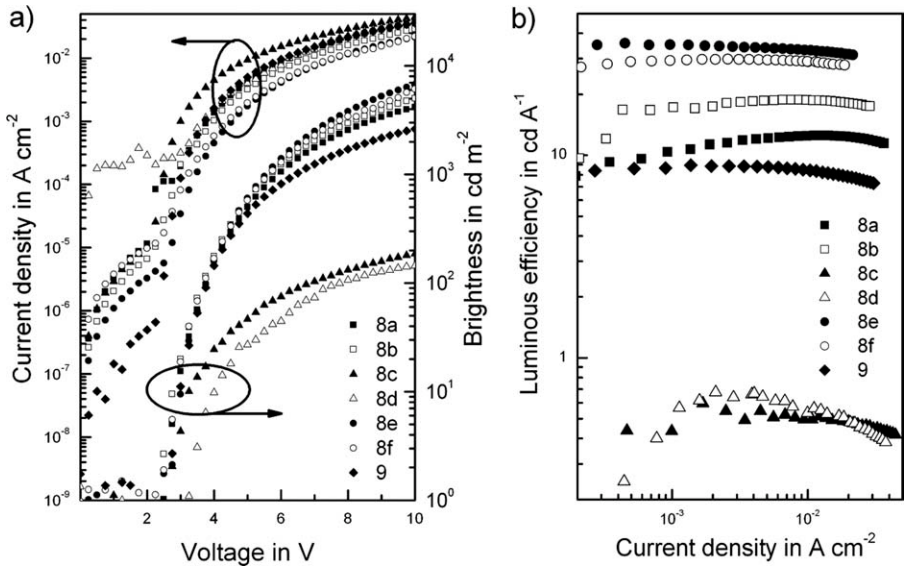

FIGURE 6 (a) Brightness and current density as function of the applied bias of polymers **8a–f** and **9** as blends with *tert*-BuPBD and Ir(Me-ppy)$_3$; (b) Luminous efficiency as a function of the current density of polymers **8a–f** and **9** as blends with *tert*-BuPBD and Ir(Me-ppy)$_3$ (polymer layer thicknesses noted in Table 3).

of the hosts **8c** and **8d** to be at 2.25 eV (551 nm) and 2.30 eV (539 nm), respectively. In Figure 7, we find the 300 K 0–0 peak of our phosphorescent emitter, Ir(Me-ppy)$_3$, to be at 2.39 eV (517 nm) with **8a** or 2.40 eV (519 nm) with **8b**. This is consistent with literature values of 2.42 eV (512 nm), and at higher energies than in the hosts **8c** and **8d**.[38] An energetic arrangement where the host triplet is at lower energy than the guest triplet is unsuitable since any triplets that still are formed on the guest may be quenched by the host. This process can further contribute to poor EL performances.

We now compare the host polymers in the first group that is **8a**, **8b**, **8e**, and **8f**. We note that the luminous efficiencies at 100 cd m^{-2} scale with the HOMO level of the host polymers. Highest efficiency is reached with **8e** that has a HOMO of −5.41 eV, followed by **8f** (−5.41 eV), **8b** (−5.08 eV), and **8a** (−5.07eV). We attribute the noticeably better performance of **8b** compared with **8a** to the additional CH_3 sidegroup that can prevent possible detrimental interchain interactions.

In summary, the polymer **8e** with the carbazolyl side groups exhibited the best overall performance with a luminous efficiency of about 35.1 cd A^{-1} at 100 cd m^{-2}. Furthermore, **8e** has a quite low current density of 0.02 A cm^{-2} at the maximum voltage of 10 V. Only the phenothiazine-functionalized polymer showed nearly similar charge transport behavior. The electroluminescence maxima for these two polymers as matrix material in this blend system are at 522 and 520 nm, respectively, and reflect the phosphorescent emission of the dopant. Because of their excellent charge transport behavior, these two polymers have been chosen for further investigations. The best device performance for **8e** and **8f** is in good relation to their measured HOMO values that allow an efficient hole transfer to the emitter described above, already.

The TPD derivative **9**, which is known to be an efficient hole-transporting matrix molecule, only shows a luminous efficiency at 100 cd m^{-2} of 8.7 cd A^{-1}. Furthermore, an exciplex formation between TPD and *tert*-BuPBD for small

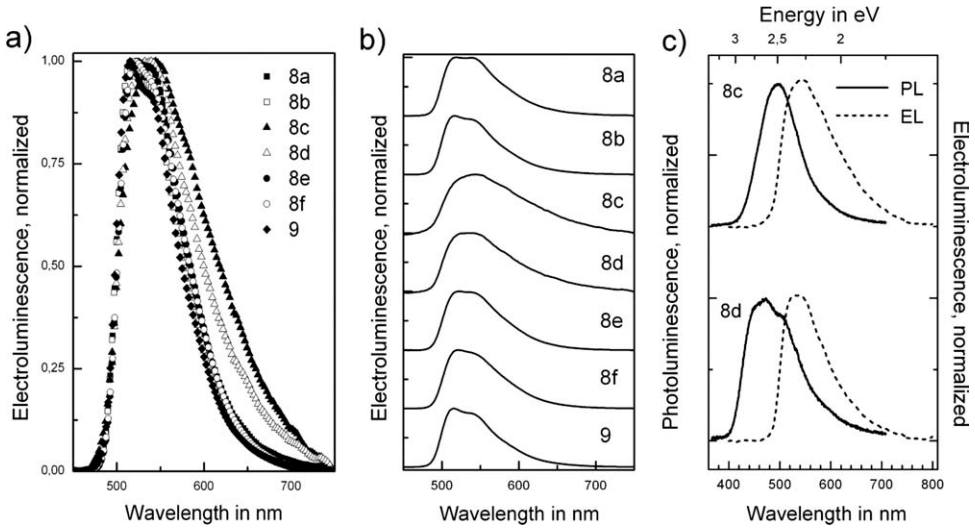

FIGURE 7 (a) Stacked, (b) superposed electroluminances of polymers **8a–f** and **9**, (c) comparison of photoluminescence of **8c** and **8d** (blended with Ir(Me-ppy)$_3$) with electroluminescence (polymer layer-thicknesses of devices noted in Table 3).

molecules has been reported before.[40] In our case, there is no broadening and no bathochromic shift observable in the emissive spectra so the maxima of emission for this device was found at 515 nm. As mentioned before, the HOMO- and LUMO-energy levels of the hole-transporting host-polymers are well matched to the energy levels of the phosphorescent dopant and the electron transporting material to obtain an efficient device, i.e., the difference in the energy levels of the host-polymers are not sufficient to interpret the different luminescent behavior of the devices. In conclusion, there has to be another reason for the difference in brightness and luminous efficiency of the TPD derivative to the carbazole-substituted polymer. Therefore, we prepared organic field effect transistors of the poly(TPD) **9** and the most promising carbazole-functionalized polymer, **8e**, to ascertain their field effect mobility. The field effect mobility of poly(TPD) **9** was found to be 1×10^{-4} cm^2 V^{-1} s^{-1} and that one of the carbazole-functionalized polymer **8e** turned out to be limited to 7×10^{-6} cm^2 V^{-1} s^{-1}. McKeown et al.[28] reported the hole mobility of **8f** to be 2×10^{-6} cm^2 V^{-1} s^{-1} and of **8a** to be 8×10^{-6} cm^2 V^{-1} s^{-1}. In addition, the mobility of *tert*-BuPBD in a polystyrene host is in the range of 4×10^{-7} to 9×10^{-7} cm^2 V^{-1} s^{-1}.[40] Based on our PLED device characteristics, we conclude that a hole mobility in the range of the poly(TPD) derivative is a limiting factor for the electronic device properties of those established blend systems. The polymers with hole mobilities in the range of 10^{-6} cm^2 V^{-1} s^{-1} (side functionalities carbazolyl, phenothiazinyl) seemed to be the better choice for efficient and bright PLED blend systems with *tert*-BuPBD and Ir(Me-ppy)$_3$, in that case. For an efficient single-layer PLED, it is of crucial importance that the charge carrier mobilities for both types of charges are in a good balance, to prevent a build-up of one charge type in the emissive layer. In small molecule devices, this challenge can be managed easily by a tuning of the different layer thicknesses. In polymer blend systems, fabricated as single layer devices, this needs to be obtained by careful variation of the blend composition. Figure 6(b) demonstrates for the device with the poly(TPD) a small efficiency roll-off initiating at higher current densities. Such an efficiency roll-off has been attributed to a triplet–triplet annihilation process between the phosphorescent dopant and the host materials.[41] For the devices with the carbazole- and phenothiazine-substituted polymers, **8e** and **8f**, respectively, the efficiency roll-off is not observable up to 20 mA cm^{-2}. The better efficiency of these polymers compared with the others is an indication for a well-balanced carrier density in the device.

It has to be mentioned that the given data concerning the electroluminescence of the prepared PLEDs do not show the maximal accessible efficiencies and luminances. Knowing that these parameters are strongly dependent on the emission layer thicknesses, only the data of comparable layer thicknesses were selected for a comparison.

CONCLUSIONS

A series of novel styrene-based monomers and their polymers have been synthesized as new hole-transporting materials for PLEDs. The polymers were characterized with respect to their EL performance in single-layer green phosphorescent PLEDs as host-polymers in blend systems. Singlet and triplet excited states of the host polymers were assigned on the basis of time- and temperature-dependent photoluminescence measurements. Triplet excited state energies in the hosts range from 2.70 to 2.25 eV, with the lower energy triplets in the naphthyl derivatives. Although the naphthyl derivatives are therefore not suitable as hosts for the green-emitting Ir(Me-ppy)$_3$, the other polymers showed very narrow emission spectra, which demonstrates; high suitability for the creation of clear colors. Two polymers turned out to be favored for further investigations, because of their excellent host behavior in such blend systems. The carbazole-substituted polymer, **8e**, is the most efficient and brightest hole-transporting polymer matrix in a blend system with *tert*-BuPBD and Ir(Me-ppy)$_3$, followed by the phenothiazine compound **8f**. This is attributed to a good balance of electron and hole mobility. Furthermore, these two polymers exhibits relatively high glass transition temperatures of >200 °C, which is a favorable property for devices with stable lifetimes. In comparison with the well-known poly(TPD), the electroluminescent behavior of the host materials **8e** and **8f** in the prepared polymer blend PLEDs is twice as good.

The authors thank the Federal Ministry of Education and Research of Germany (BMBF) for financial support within the CARO project (01 BD 0685) and (01 BD 0687). The authors thank Steffi Kreissl for device preparation and Tatjana Egorov-Brening for OFET preparation.

REFERENCES AND NOTES

1 Burroughes, J. H.; Bradley, D. D. C.; Brown, A. R.; Marks, R. N.; Mackay, K.; Friend, R. H.; Burns, P. L.; Holmes, A. B. Nature 1990, 347, 539.

2 Hebner, T. R.; Wu, C. C.; Marcy, D.; Lu, M. H.; Sturm, J. C. Appl Phys Lett 1998, 72, 1998.

3 de Gans, B.-J.; Duineveld, P. C.; Schubert, U. S. Adv Mater 2004, 16, 203.

4 Joo, C. W.; Jeon, S. O.; Yook, K. S.; Lee, J. Y. Org Electron 2009, 10, 372.

5 Tuomikoski, M.; Suhonen, R.; Välimäki, M.; Maaninen, T.; Maaninen, A.; Sauer, M.; Rofin, P.; Menning, M.; Heusing, S.; Puetz, J.; Aegerter, M. A. Proc SPIE 2006, 6192, 619204.

6 Adachi, C.; Baldo, M. A.; Thompson, M. E.; Forrest, S. R. J Appl Phys 2001, 90, 5048.

7 Köhler, A.; Bässler, H. Mater Sci Eng R 2009, 66, 71.

8 Chen, X.; Liao, J.-L.; Liang, Y.; Ahmed, M. O.; Tseng, H.-E.; Chen, S.-A. J Am Chem Soc 2003, 125, 636.

9 Sandee, A. J.; Williams, C. K.; Evans, N. R.; Davies, J. E.; Boothby, C. E.; Köhler, A.; Friend, R. H.; Holmes, A. B. J Am Chem Soc 2004, 126, 7041.

10 Gong, X.; Ostrowski, J. C.; Bazan, G. C.; Moses, D.; Heeger, A. J.; Liu, M. S.; Jen, A. K.-Y. Adv Mater 2003, 15, 45.

11 Al Attar, H. A.; Monkman, A. P.; Tavasli, M.; Bettington, S.; Bryce, M. R. Appl Phys Lett 2005, 86, 121101.

12 Doi, S.; Sekine, C.; Tsubata, Y.; Ueda, M.; Noguchi, T.; Ohnishi, T. J Photopolym Sci Technol 2003, 16, 303.

13 Baldo, M. A.; Thompson, M. E.; Forrest, S. R. Nature 2000, 403, 750.

14 Tong, B.; Mei, Q.; Wang, S.; Fang, Y.; Meng, Y.; Wang, B. J Mater Chem 2008, 18, 1636.

15 De Angelis, F.; Fantacci, S.; Evans, N.; Klein, C.; Zakeeruddin, S. M.; Moser, J.-E.; Kalyanasundaram, K.; Bolink, H. J.; Grätzel, M.; Nazeeruddin, M. K. Inorg Chem 2007, 46, 5989.

16 You, Y.; Park, S. Y. Dalton Trans 2009, 8, 1267.

17 Gong, X.; Lim, S.-H.; Ostrowski, J. C.; Moses, D.; Bardeen, C. J.; Bazan, G. C. J Appl Phys 2004, 95, 948.

18 Tokito, S.; Suzuki, M.; Sato, F.; Kamachi, M.; Shirane, K. Org Electron 2003, 4, 105.

19 Yang, X. H.; Neher, D. Appl Phys Lett 2004, 84, 2476.

20 Yang, X.; Müller, D. C.; Neher, D.; Meerholz, K. Adv Mater 2006, 18, 948.

21 Kawamura, Y.; Yanagida, S.; Forrest, S. R. J Appl Phys 2002, 92, 87.

22 Park, J. J.; Park, T. J.; Jeon, W. S.; Pode, R.; Jang, J.; Kwon, J. H.; Yu, E.-S.; Chae, M. Y. Org Electron 2009, 10, 189.

23 Adachi, C., Nagai, K.; Tamoto, N. Appl Phys Lett 1995, 66, 2679.

24 Tokito, S.; Tanaka, H.; Noda, K.; Okada, A.; Taga, Y. Appl Phys Lett 1997, 70, 1929.

25 Shirota, Y.; Kuwabara, Y.; Okuda, D.; Okuda, R.; Ogawa, H.; Inada, H.; Wakimoto, T.; Nakada, H.; Yonemoto, Y.; Kawami, S.; Imai, K. J Lumin 1997, 72-74, 985.

26 Suzuki, M.; Tokito, S.; Sato, F.; Igarashi, T.; Kondo, K.; Ymaguchi, T. Appl Phys Lett 2005, 86, 103507.

27 Thesen, M. W.; Krueger, H.; Janietz, S.; Wedel, A.; Graf, M. J Polym Sci Polym Chem 2010, 48, 389.

28 McKeown, N. B.; Badriya, S.; Helliwell, M.; Shkunov, M. J Mater Chem 2007, 20, 2088.

29 Debeaux, M.; Thesen, M. W.; Schneidenbach, D.; Hopf, H.; Janietz, S.; Krueger, H.; Wedel, A.; Kowalsky, W.; Johannes, H.-H. Adv Funct Mater 2010, 20, 399.

30 de Mello, J. C.; Wittmann, H. F.; Friend, R. H. Adv Mater 1997, 9, 230.

31 Wilson, J. S.; Chawdhury, N.; Al-Mandhary, M. R. A.; Younus, M.; Khan, M. S.; Raithby, P. R.; Kohler, A.; Friend, R. H. J Am Chem Soc 2001, 123, 9412.

32 Pope, M.; Swenberg, C. E. Electronic Processes in Organic Crystals and Polymers, 2nd ed.; Oxford Science Publications: Oxford, 1999; p 32.

33 Wang, D.; Li, W.; Chu, B.; Su, Z.; Bi, D.; Zhang, D.; Zhu, J.; Yan, F.; Chen, Y.; Tsuboi, T. Appl Phys Lett 2008, 92, 053304.

34 Meyer, J.; Hamwi, S.; Bülow, T.; Johannes, H.-H.; Riedl, T.; Kowalsky, W. Appl Phys Lett 2007, 91, 113506.

35 Lim, J. T.; Jeong, C. H.; Lee, J. H.; Yeom, G. Y.; Jeong, H. K.; Chai, S. Y.; Lee, I. M.; Lee, W. I. J Organomet Chem 2006, 691, 2701.

36 Kondakova, M. E.; Deaton, J. C.; Pawlik, T. D.; Giesen, D. J.; Kondakov, D. Y.; Young, R. H.; Royster, T. L., Comfort, D. L.; Shore, J. D. J Appl Phys 2010, 107, 014515.

37 Shirota, Y.; Kuwabara, Y.; Inada, H.; Wakimoto, T.; Nakada, H.; Yonemoto, Y.; Kawami, S.; Imai, K. Appl Phys Lett 1994, 65, 807.

38 Wu, H.; Zou, J.; Liu, F.; Wang, L.; Mikhailovsky, A.; Bazan, G. C.; Yang, W.; Cao, Y. Adv Mater 2008, 20, 696.

39 Kolosov, D.; Adamovich, V.; Djurovich, P.; Thompson, M. E.; Adachi, C. J Am Chem Soc 2002, 124, 9945.

40 Tameev, A. R.; He, Z.; Milburn, H. W.; Kozlov, A. A.; Vannikov, A. V.; Puchala, A.; Rasala, D. Appl Phys Lett 2002, 81, 969.

41 Baldo, M. A.; Adachi, C.; Forrest, S. R. Phys Rev B 2000, 62, 10967.